WARSAW UNIVERSITY OF TECHNOLOGY Index 351733
FACULTY OF CIVIL ENGINEERING
COMMITTEE FOR CIVIL AND WATER ENGINEERING
POLISH ACADEMY OF SCIENCES ISSN 1230-2945

DOI: 10.24425/ace.2025.153340

ARCHIVES OF CIVIL ENGINEERING

Vol. LXXI ISSUE 1 2025

pp. 381 –401

Research paper

Experimental and numerical verification of the standard procedure for determining the load capacity of GFRP composite lighting columns

Mirosław Broniewicz[1], Filip Broniewicz[2], Elżbieta Broniewicz[3]

Abstract: The main objective of the research was to validate the method for determining the load capacity of GFRP composite lighting columns under horizontal loads according to the EN 40-3-3:2013 standard. The work involved developing a numerical model of GFRP composite columns with an inspection hole while accounting for the columns' nonlinear behaviour before the failure phase. The model was verified by testing 11 GFRP lighting columns on a natural scale and material testing of the composite. A calculation method was used in accordance with the standards EN 40-3-3:2013 and EN-40-7:2002 to determine their bending resistance. It was discovered that the load capacity estimated experimentally is two to three times less than the load capacity estimated using the standard's procedure. Also, the load capacity calculated based on the developed numerical model of the column is about 2.5 times lower than the characteristic load capacity calculated based on the currently applicable standard procedure. The analysis of the standard design procedure shows that the inspection opening is treated only as a local reduction of the cross-section, reducing the yield modulus. However, the possibility of buckling the walls in the inspection opening area is not taken into account. It means that the standard procedure for determining the bending resistance of composite columns has not been adapted to the actual behaviour of composite columns with inspection openings. Developed numerical model of a lighting pole with an unreinforced inspection opening accurately assesses the capacity of such poles for use in scientific and design practice.

Keywords: composite structures, design procedure, experimental investigation, FEM analysis, GFRP lighting poles, flexural behaviour

[1]DSc., Eng., PB Prof., Bialystok University of Technology, Faculty of Civil Engineering and Environmental Sciences, Wiejska St. 45A, 15-351 Bialystok, Poland, e-mail: m.broniewicz@pb.edu.pl, ORCID: 0000-0001-8267-6095
[2]MSc., Eng., Bialystok University of Technology, Faculty of Civil Engineering and Environmental Sciences, Wiejska St. 45A, 15-351 Bialystok, Poland, e-mail: f.broniewicz@doktoranci.pb.edu.pl, ORCID: 0000-0003-4506-5521
[3]DSc., Eng., PB Prof., Bialystok University of Technology, Faculty of Civil Engineering and Environmental Sciences, Wiejska St. 45A, 15-351 Bialystok, Poland, e-mail: e.broniewicz@pb.edu.pl, ORCID: 0000-0002-9231-2225

1. Introduction

It was necessary to introduce new, secure, and environmentally friendly technological and material solutions in response to the increasing demand for column load-bearing structures in the energy, road, and railway industries that better functional properties would distinguish. Traditional building materials, like wood, steel and concrete, which have been used for many years to construct transmission and lighting poles, only partially meet the criteria for sustainable development and environmental preservation [1]. Over the last 25 years, significant progress has been made in introducing lighting and transmission poles made of polymer composites reinforced with various fibres (FRP) to the energy market. FRP fibre-reinforced composite poles represent a modern engineering solution where sustainability plays an important role (Fig. 1).

Fig. 1. Composite circular GFRP lighting poles [2]

Although FRP composite materials have many advantages and progress is being made towards their widespread use in many areas of the economy, composite structures are still not well recognised in strength and utility [3]. There are no design guidelines and standards that would cover various types of composite elements, not only with the basic shapes indicated in the currently existing subject standards but also with other shapes and dimensions, with reinforced and unreinforced openings in the shafts of columns. In order to facilitate and popularise the use of fibre-reinforced composite poles and accelerate the process of approval and implementation in the energy infrastructure of this type of product, end-users of the product should better understand all aspects related to the design and use of FRP composite poles. Experimental studies of GFRP composite lighting poles show a significant overestimation of the design load capacity, determined based on currently applicable European standards. Therefore, there is an urgent need to verify the existing calculation procedures experimentally, indicated in the standards, both in determining the design resistance of columns to bending and the deflection value.

In order to evaluate the strength and deformation characteristics of composite columns reinforced with glass fibre GFRP, an experimental programme was started and carried out [4]. This program's goal was to use experimental and numerical FEM verification to validate the standard calculation method for composite conical GFRP columns with a circular cross-section and an inspection hole in the lower part of the shaft. Following experimental tests of the bending load capacity of composite columns in their natural state, the program's first stage involved determining the standard load capacity of lighting composite columns in accordance with EN 40-3-3 [5].

The first studies on the buckling capacity of composite columns without inspection holes were carried out at West Virginia University in the USA in the 1990s by Barbero and Raftoyiannis [6]. Analysing the behaviour of composite columns under the influence of axial load, they found that from a mathematical point of view, there is an infinite number of buckling loads, each of which is associated with a specific form of loss of general stability, confirming the validity of Euler's theory in relation to composite elements.

Zhi-Min Lin experimentally investigated the behaviour of FRP composite transmission poles [7]. The columns were fixed in a cantilever manner and loaded with a transverse force applied to the top of the column. During the tests, it was observed that the columns were damaged in the two most critical places, in the vicinity of the inspection hole and in the place where the composite column shaft was connected to the steel footing. The test results showed that the stiffness and strength of the FRP columns and the method of their failure depend mainly on the thickness of the walls. In the case of shafts with a smaller thickness, the columns were destroyed as a result of local loss of stability at the site of the inspection hole. In contrast, in the case of greater wall thicknesses, the dominant form of destruction exceeded the strength of the material at the base.

Another study on composite poles was conducted at the University of Manitoba, Canada [8]. Strength issues of composite lighting columns in the shape of a truncated cone made by the filament winding method were analysed. It has been shown that the dynamic properties depend mainly on the ratio of the upper and lower column diameters and the angle of the reinforcement fibres. They demonstrated by comparing the results of FEM numerical tests with the experimental tests carried out that their computational model perfectly presents the behaviour of columns under the applied load and allows for good prediction of the critical force.

In 2007, researchers from the University of Sherbrooke [9] analysed the behaviour of GFRP columns loaded with shear force. Twenty-three columns shaped like a truncated cone with 5 to 12 meters in length were tested. The results of the tests showed that the deflection of the column end is linearly dependent on the load in its entire range, and the failure occurred as a result of the column's loss of stability in the compression zone. The presence of an inspection hole without additional reinforcement reduces the strength and flexural stiffness of the column and is a critical point where GFRP columns fail. It was not found that the distance of the inspection opening from the base and covering the inspection opening with a special cover had a significant impact on the strength of the column.

The behaviour of thin-walled flat plates with a central cutout under uniform compression was studied by the authors and presented in [10]. They discovered good agreement between the FEM numerical method and the Koiter's and straight-lines intersection approximation methods

by figuring out the slab's critical load. Additionally, they conducted a nonlinear analysis of the structure using an initiated geometric imperfection that matched the plate's flexural-torsion buckling mode. The developed numerical model of the structure was shown to be accurate when the numerical results were compared with experimental results.

A summary of the review of research on FRP composite elements allows the following conclusions to be drawn:

1. There is a strict dependence of the composite material on the strength of the components of its structure, i.e. reinforcing fibers and resin.
2. Significant differences were found in the capacity of composite elements between the experimental test results and theoretical estimates, resulting from the initial geometric and material imperfections, the method of applying the load and degree of restraint the ends of the tested elements.
3. In the case of composite elements with slender walls, before the material strength is achieved, the element is destroyed due to local loss of stability.
4. Columns with an inspection opening fail at the location of the opening, while in the case of large wall thicknesses, the dominant form of failure is when the strength of the material at the base of the column is exceeded.
5. FEM numerical models well reproduce the behavior of composite elements and are the right tool for determining the critical load.

2. Calculation of GFRP lighting columns' load capacities in accordance with the relevant standards

Requirements related to the design and computational verification of composite lighting columns were presented in the standard [5]. They concern the determination of the properties of columns, including the ultimate limit state and the serviceability limit state. According to the standard's requirements, the column's bending capacity should be checked in three critical cross-sections, i.e. at the point of attachment of the column, at the lower edge of the inspection opening and at the upper edge of the inspection opening.

The strength of lighting columns should be determined, taking into account the cross-sectional features giving the lowest values of the bending load capacity. The verification of the bending resistance of the column was carried out according to [5], taking into account the amendments contained in [12]. The characteristic strength of the material of the lighting columns made of polymer composites was determined according to [13]. The mechanical properties of the composite material taken from the tested elements were determined on the basis of tests carried out on the Zwick Roell BPS-HP004 machine, including the determination of mechanical properties during static tension of fiber-reinforced composites and a bending test (Fig. 2).

The characteristic load of the columns was calculated according to the standard's requirements [12].

Bending resistances in critical sections of 3 m high columns are shown in Table 1.

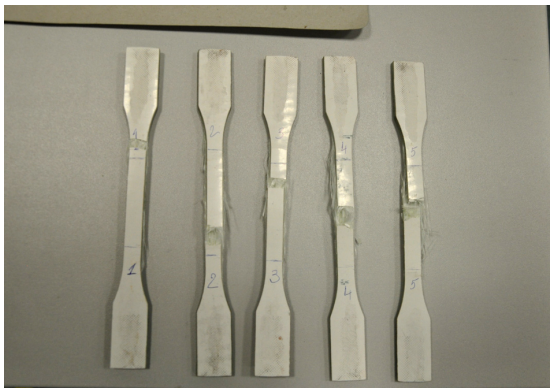

Fig. 2. View of the samples after a static tensile test

Table 1. Bending resistance of critical sections of columns with a height of 3 m

Column number		**Column 3/1 (h = 3.0)**	**Column 3/2 (h = 3.0)**	**Column 3/3 (h = 3.0)**
Material properties	**f_y = 229.0 MPa**	**E = 18948 MPa**	**G = 7177.3 MPa**	**v = 0.32**
Bending resistance at the base				
Geometric parameters		d_{b1} = 128.3 m	d_{b2} = 127.1 m	d_{b3} = 127.7 m
		r_{b1} = 64.2 m	r_{b2} = 63.6 m	r_{b3} = 63.9 m
		t_{b1} = 4.1 m	t_{b2} = 3.9 m	t_{b3} = 4.3 m
$Z_p = 4 \cdot R^2 \cdot t$		$6.75 \cdot 10^4$ m^3	$6.30 \cdot 10^4$ m^3	$7.01 \cdot 10^4$ m^3
$\varepsilon = \frac{R}{t}\sqrt{\frac{f_y}{E}}$		1.72	1.79	1.63
$K = \left[2\left[1+\nu_{12}\left(\frac{E_2}{E_1}\right)^{\frac{1}{2}}\right]\left(\frac{E_2}{E_1}\right)^{\frac{1}{2}} \cdot \left(\frac{G}{E_1}\right)^{\frac{1}{2}}\right]^{\frac{1}{2}}$		1.27	1.27	1.27
$\phi_1 = K\left(\frac{0.8}{\varepsilon}\right)^{0.35}$		0.975	0.961	0.993
$M_{up} = \frac{f_y \cdot \phi_1 \cdot Z_p}{\gamma_m}$		10047 N·m	9246 N·m	10631 N·m
Bending resistance at the lower edge of the inspection hole				
Geometric parameters		d_{hb1} = 125.4 mm	d_{hb2} = 124.4 mm	d_{hb3} = 125.4 mm
		r_{hb1} = 62.7 mm	r_{hb2} = 62.2 mm	r_{hb3} = 62.7 mm
		t_{hb1} = 4.0 mm	t_{hb2} = 3.8 mm	t_{hb3} = 4.3 mm
$Z_{pn} = 2 \cdot F \cdot R^2 \cdot t \cdot \cos\frac{\theta}{2} \cdot \left(1 - \sin\frac{\theta}{2}\right)$		$4.08 \cdot 10^4$ mm^3	$3.79 \cdot 10^4$ mm^3	$4.38 \cdot 10^4$ mm^3
$Z_{py} = FR^2t(1+\cos\theta)$		$6.13 \cdot 10^4$ mm^3	$5.73 \cdot 10^4$ mm^3	$6.59 \cdot 10^4$ mm^3

Continued on next page

Table 1 – *Continued from previous page*

Column number		**Column 3/1 (h = 3.0)**	**Column 3/2 (h = 3.0)**	**Column 3/3 (h = 3.0)**
Material properties	**f_y = 229.0 MPa**	**E = 18948 MPa**	**G = 7177.3 MPa**	**v = 0.32**
$\varepsilon = \frac{R}{t}\sqrt{\frac{f_y}{E}}$		1.72	1.80	1.60
$\phi_1 = K \cdot \left(\frac{0.8}{\varepsilon}\right)^{0.35}$		0.974	0.960	0.999
$\phi_3 = \frac{t^2 E}{t^2 E + 0.07 R L f_y}$		0.611	0.588	0.645
$M_{ux} = \frac{f_y \cdot g \cdot \phi_3 \cdot Z_{pn}}{\gamma_m}$		3805 N·m	3408 N·m	4317 N·m
$M_{uy} = \frac{f_y \cdot g \cdot \phi_3 \cdot Z_{py}}{\gamma_m}$		5718 N·m	5145 N·m	6487 N·m
Bending resistance in the middle of the height of the inspection hole				
Geometric parameters		d_{hm1} = 125.0 mm	d_{hm2} = 124.0 mm	d_{hm3} = 125.1 mm
		r_{hm1} = 62.5 mm	r_{hm2} = 62.0 mm	r_{hm3} = 62.5 mm
		t_{hm1} = 4.0 mm	t_{hm2} = 3.8 mm	t_{hm3} = 4.0 mm
Z_{pn}		$4.04 \cdot 10^4$ mm^3	3.7510^4 mm^3	$4.05 \cdot 10^4$ mm^3
Z_{py}		$6.09 \cdot 10^4$ mm^3	$5.69 \cdot 10^4$ mm^3	$6.10 \cdot 10^4$ mm^3
ε		1.72	1.79	1.60
ϕ_1		0.976	0.961	0.975
ϕ_3		0.612	0.595	0.613
M_{ux}		3778 N·m	3410 N·m	3786 N·m
M_{uy}		5688 N·m	5166 N·m	5706 N·m
Bending resistance at the top edge of the inspection hole				
Geometric parameters		d_{ht1} = 124.6 mm	d_{ht2} = 123.6 mm	d_{ht3} = 124.7 mm
		r_{ht1} = 62.3 mm	r_{ht2} = 61.8 mm	r_{ht3} = 62.4 mm
		t_{ht1} = 4.0 mm	t_{ht2} = 3.8 mm	t_{ht3} = 4.3 mm
Z_{pn}		$4.01 \cdot 10^4$ mm^3	$3.72 \cdot 10^4$ mm^3	$4.31\ 10^4$ mm^3
Z_{py}		$6.05 \cdot 10^4$ mm^3	$5.65 \cdot 10^4$ mm^3	$6.51 \cdot 10^4$ mm^3
ε		1.71	1.79	1.59
ϕ_1 =		0.977	0.962	1.001
ϕ_3 =		0.613	0.596	0.647
M_{ux}		3750 N·m	3385 N·m	4262 N·m
M_{uy} =		5657 N·m	5139 N·m	6436 N·m

Checking the bending resistance of columns with a height of 3.0 m, 5.0 m, 7.0 m and 9.0 m at the base of the column and in the middle of the height of the inspection opening is presented in Table 2.

Table 2. Checking the bending resistance

Formula	Pole x/1	Pole x/2	Pole x/3
Poles 3 m high (3/1,3/2, 3/3)			
Bending resistance at the base			
$\boldsymbol{M_{up} = \frac{f_y \cdot \phi_1 \cdot Z_p}{\gamma_m}}$	M_{up} = 10059.6 N·m	M_{up} = 9246.3 N·m	M_{up} = 10631.3 N·m
$M_p = \sqrt{M_x^2 + M_y^2}$	722.5 N·m	722.5 N·m	722.5 N·m
M_p / M_{up}	0.07	0.08	0.07
Bending resistance at the inspection opening			
$\boldsymbol{M_{u(x.y)} = \frac{f_y \cdot g \cdot \phi_3 \cdot Z_{p(x.y)}}{\gamma_m}}$	M_{ux} = 3666.9 N·m	M_{ux} = 3331.6 N·m	M_{ux} = 4169.3 N·m
	M_{uy} = 5188.8 N·m	M_{uy} = 4714.3 N·m	M_{uy} = 5899.7 N·m
$\frac{M_x}{M_{ux}} + \frac{M_y}{M_{uy}}$	0.13	0.14	0.11
Poles 5 m high (5/1, 5/2, 5/3)			
Bending resistance at the base			
M_p / M_{up}	0.11	0.12	0.12
Bending resistance at the inspection opening			
$\frac{M_x}{M_{ux}} + \frac{M_y}{M_{uy}}$	0.33	0.34	0.33
Poles 7 m high (7/1, 7/2, 7/3)			
Bending resistance at the base			
M_p / M_{up}	0.10	0.11	0.12
Bending resistance at the inspection opening			
$\frac{M_x}{M_{ux}} + \frac{M_y}{M_{uy}}$	0.24	0.30	0.30
Poles 9 m high (9/1, 9/2)			
Bending resistance at the base			
M_p / M_{up}	0.18	0.20	–
Bending resistance at the inspection opening			
$\frac{M_x}{M_{ux}} + \frac{M_y}{M_{uy}}$	0.48	0.51	–

Table 2 illustrates that the bending capacity of the tested columns at the base was utilized in 7% for columns that were 3.0 m high and in 20% for columns that were 9.0 m high. For columns that are 3.0 meters high or more, the utilization of the columns' capacity in the location of the opening varies from 0.11 to 0.51.

3. Experimental research of GFRP lighting poles

The tests' objectives were to gather experimental information on the stiffness and load capacity of GFRP composite columns subjected to static loads and to investigate experimentally the phenomenon of column wall stability loss close to the inspection opening.

The research covered composite poles currently manufactured in Poland, intended for the construction of lighting and transmission lines. The pultrusion method, which produces composite profiles in a variety of shapes, including solid, open, and closed, was used to create the tested columns. Since the fibres are oriented unidirectionally in this instance, high values of mechanical parameters (tensile strength and elastic modulus) can be achieved in the fibres' direction. These values are substantially lower in directions that are transverse to the fibre direction.

The standard [13] outlines the requirements for designing and testing lighting columns made of polymer composites reinforced with glass fibre. This standard covers lighting poles with a nominal height of no more than 20 m. Eleven lighting poles with the following lengths were included in the test plan: 3.0 m – 3 pieces, 5.0 m – 3 pieces, 7.0 m – 3 pieces, and 9.0 m – 2 pieces. Table 3 presents the test columns' geometrical measurements.

The test stand was set up in compliance with EN 40-3-2 [13] guidelines. It consisted of a 600 × 800 support block, a load application system, a bearing-equipped strip, and a stress measurement system for the column (Fig. 3).

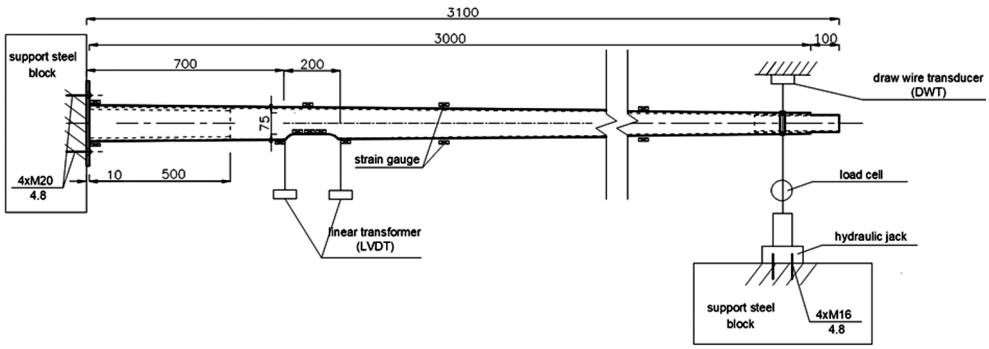

Fig. 3. Schematic drawing of the full-scale test setup for 3.0 m poles

The end support was based on sliding bearings, which eliminated the friction between the surface of the column and the support. Single-segment columns without reinforcement around the inspection hole made up all of the tested units. The poles were constructed from a composite of polyester resin and E-glass fibre. The inspection holes were made during the production

Table 3. List of geometrical dimensions of test elements

Column No	Column height [mm]	Diameter base/top [mm]	Wall thickness at the base [mm]	Inspection hole		
				Dimensions [mm]	Distance from the base [mm]	Location of the hole on the side
3/1	3001	128.3/73.6	4.1	200.5 × 75.3	703	compresion
3/2	3002	127.1/72.6	3.9	196.0 × 75.5	704	compresion
3/3	2992	127.7/73.9	4.3	199.5 × 75.5	703	compresion
5/1	4999	147.1/72.6	4.3	299.0 × 85.6	604	compresion
5/2	5001	147.8/73.9	4.2	308.0 × 85.1	606	compresion
5/3	5003	146.8/72.9	4.2	299.0 × 82.8	605	compresion
7/1	7003	195.5/73.6	5.6	408.0 × 85.5	706	compresion
7/2	7004	194.6/73.9	5.1	398.0 × 84.5	704	compresion
7/3	7003	195.9/72.6	5.0	408.0 × 85.4	703	compresion
9/1	8941	198.7/72.9	5.4	404.0 × 85.1	703	compresion
9/2	8950	198.1/74.2	5.3	404.0 × 85.5	703	compresion

of the poles. S235JR steel, which has a tensile strength of 360 MPa and a yield strength of 235 MPa, is used to construct the base plates of GFRP lighting columns. Dimensions of the base's horizontal plate were 295 × 295 × 10 mm. A fillet weld with a thickness of 4 mm was used to join a stub made of a steel pipe measuring 114.3 × 4 mm and 500 mm in length to the sheet. There were 200 mm-spaced holes for anchor bolts with a diameter of 22 mm in the base's horizontal sheet. S355 steel M20 plate anchors are available to secure the column to the foundation. Figure 4 depicts the column's view on the test stand.

Experimental tests of elements under bending load were carried out using the following measuring equipment: electro resistant foil strain gauges type TFs-5/120 with a measuring base of 8.2 mm, glued to the column shaft in the immediate vicinity of the edge of the inspection opening, a Bosch DLE40 laser rangefinder with a measurement accuracy of 0, 5 mm, used to measure the displacement of the top of the pole, TEM measuring device with legalization and calibration certificate with a maximum load of 500 kg and an accuracy of 200 g, used to measure the lateral force loading the pole, Kraft&Dele electric winch model KD1564 with a maximum lifting capacity of 4.3T, controlled by using a wireless remote control to set the load.

Strain gauges were installed on the compression side of the columns, on the external and internal surface of the wall around the inspection opening, and on the tension side, opposite

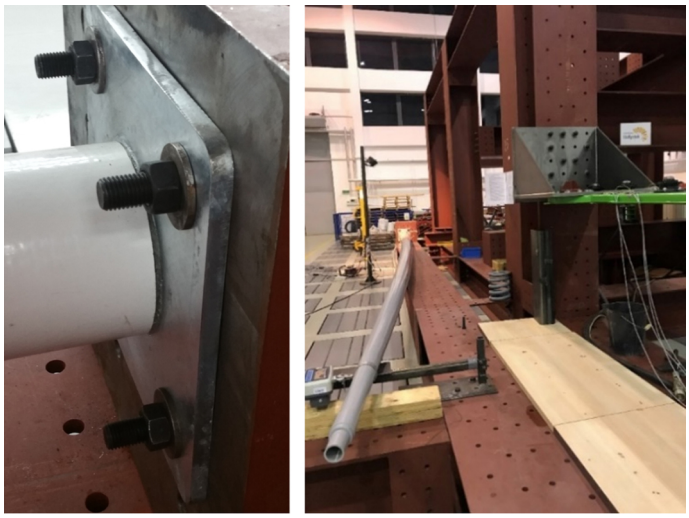

Fig. 4. View of the pole on the test stand

the opening. Three strain gauges were glued in each place to measure deformations in the longitudinal, circumferential and 45-degree directions (Fig. 5).

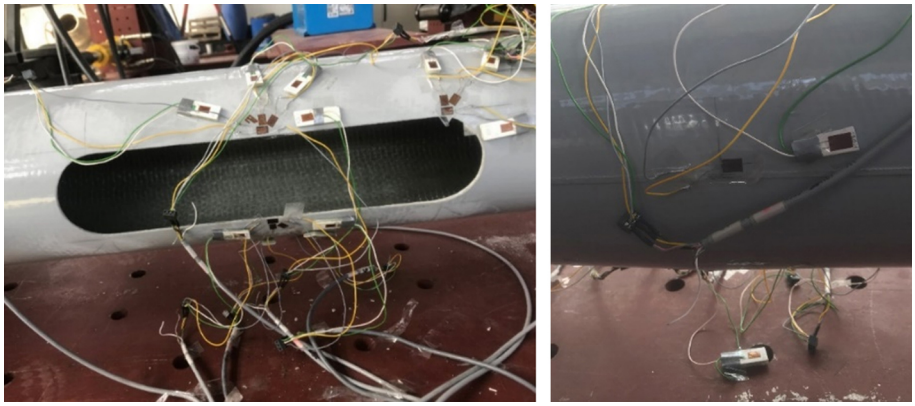

Fig. 5. Arrangement of measuring strain gauges

The load on the column was a transverse force applied using a tensioning device in accordance with the requirements of the standard [13] at a distance of 0.5 m from the top of the column. The column was loaded gradually, reading its displacement after each step up to the value of the critical load (until destruction), and the horizontal deflection and strain gauge readings were recorded. The behaviour of the column shaft in the area of the inspection hole, at the base, in the area outside the inspection hole and the loss of local stability as a result of cross-section ovalisation were observed.

Before performing the tests, the poles were each loaded and unloaded with a force of 40% of the test load (approximately 200 N) in order to eliminate any slack in the test system. The device for measuring the value of the applied force was placed between the tensioning device and the pole. The column was loaded gradually, with its displacement read after each step, up to the critical load value (until failure), and the horizontal deflection and strain gauge readings were recorded. After the column was destroyed, the permanent deformation of the end of the column and the critical force of local buckling were recorded, after which the column no longer returned to its original shape (Fig. 6).

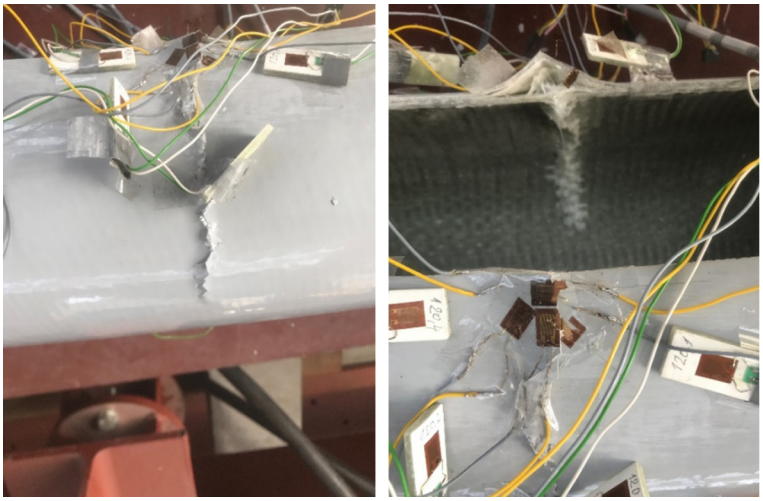

Fig. 6. Destruction of the pole in the vicinity of the inspection hole

Table 4 presents the findings from the experimental investigations of the examined elements.

Four forms of column destruction were analysed: 1 – damage in the area of the inspection hole, 2 – damage to the shaft at the base, 3 – damage to the shaft in the area outside the inspection hole, and 4 – ovalisation of the column shaft. In all the tested columns, the same form of column failure occurred, consisting of the shank cracking in the area of the inspection opening (destruction form 1).

A static equilibrium path was used to describe the behaviour of the tested columns, described in the coordinate system: loading force F and column end deflection Δ. The recorded $F - \Delta$ relationships for the 3 m column are shown in Fig. 7.

The graphs also show the equations of straight lines approximating the course of the graphs and the values of the coefficient of determination R^2, showing that the equations fit the graph (R^2 value close to one). The course of the equilibrium path and the linear form of the straight line mapping the graphs testify to the elastic behaviour of the columns during their loading until failure. Based on the diagrams, the columns' stiffness and ultimate load capacity were determined. The stiffness Sj was determined as the tangent of the inclination angle of the approximation line.

Table 4. Results of experimental studies

No. of column	Critical force $F_{cr.exp}$ [N]	Base of column		Inspection hole		Deflection pole end Δ [mm]	Directional coefficient (initial stiffness) $S_{j.ini}$	Inclination angle curve [°]	Form of destruction
		Arm force action $l_{(base)}$ [mm]	Critical moment $M_{cr(base)}$ [Nmm]	Arm force action $l_{(hole)}$ [mm]	Critical moment $M_{cr(hole)}$ [Nmm]				
3/1	987	2501	2468487	1698	1675926	122 mm	s7.326	82.23	1
3/2	903	2502	2259306	1700	1535100	137 mm	7.429	82.34	1
3/3	956	2492	2382352	1689	1614684	128 mm	7.251	82.15	1
5/1	545	4499	2451955	3746	2041570	209 mm	2.629	69.18	1
5/2	638	4501	2871638	3741	2386758	253 mm	2.694	69.64	1
5/3	664	4503	2989992	3749	2489336	218 mm	2.916	71.08	1
7/1	1179	6503	7667037	5593	6594147	436 mm	2.705	69.72	1
7/2	1114	6504	7245456	5601	6239514	444 mm	2.439	67.71	1
7/3	1158	6503	7530474	5596	6480168	459 mm	2.488	68.11	1
9/1	849	8441	7166409	7536	6398064	664 mm	1.259	51.54	1
9/2	1028	8450	8686600	7545	7756260	751 mm	1.440	55.23	1

Form of destruction: 1 – damage to the column shaft in the area around the inspection hole.

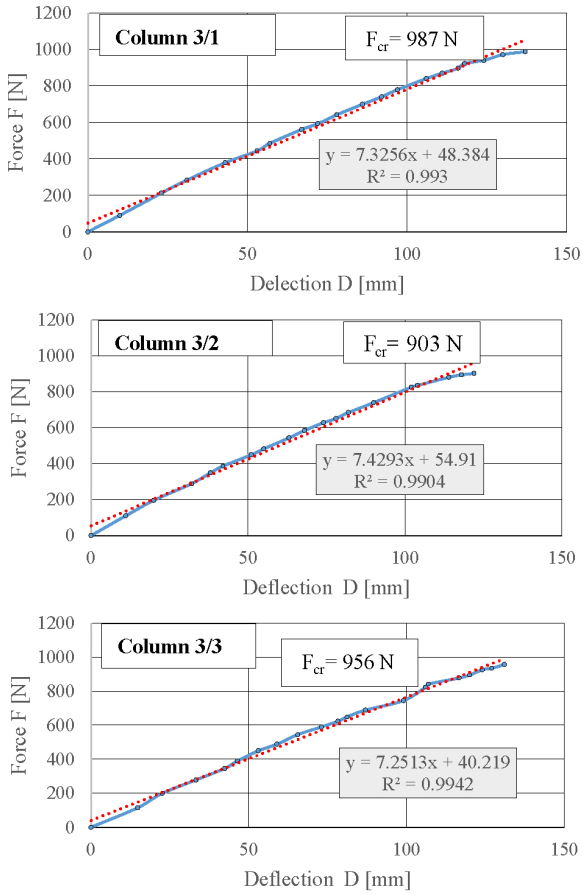

Fig. 7. Static balance paths ($F - \Delta$) columns 3.0 m high

4. Construction and validation of the FEM model

The numerical models were created in the ANSYS Structure programme, using the data from the experimental tests of the columns and material tests. A shell column model was selected as the geometry type. It consisted of a pole shaft shaped like a truncated cone with a mapped inspection hole. The increase in the stiffness of the lower part of the column caused by its fastening on the steel flange was modelled by increasing the thickness of the shaft coating in the section from 0 to 1 m from the base of the column. The SHELL 181 element was adopted as the finite element type. It is an element intended for the analysis of thin-layered shells. It has four nodes located in the corners of the element, each of which has 6 degrees of freedom: three degrees of translation u_X, u_Y, u_Z and three degrees of rotation $\theta_X, \theta_Y, \theta_Z$. The SHELL 181 element can be used especially for modelling composite coatings consisting of several or a dozen reinforcing layers of glass fibre [14]. By entering the layer thickness, material type, and

number of integration points, the SHELL 181 element allowed the definition of a multi-layer shell of the examined columns. The calculations were based on the Reissner-Mindlin first-order shear deformation theory of moderately thick coatings [15], which ensured the accuracy of the representation of composite materials. Five integration points between the layers were assumed in the calculations due to the material's plasticity. The pole is made of a laminate consisting of polyester resin and glass fibre composite layers. Material tests produced the data required to model the material forming the columns. The material exhibited isotropic characteristics in the laminate's plane. It had a constant modulus of elasticity and was linearly elastic. Due to the material's layered structure, a laminate model was created with the ability to analyse strain and stress at the level of a single layer. The laminate was made using the ACP module of the ANSYS programme. It enabled the material to be modelled in a way that made it possible to replicate the actual layer arrangement in the laminate forming the pole (Table 5).

Table 5. Arrangement of laminate layers of the tested columns

Composite type	1	2
Laminate type	[90/0 /90/0/90]	$[90/0\ /90/0/90]_T$
Number of layers	5	10

The stresses obtained from strain gauge tests were modeled in the program as normal stresses, the direction of which coincided with the strain gauge axes. In the vicinity of the inspection hole, a smaller finite element size was used than the size of the strain gauges used, therefore the average stresses from an area the size of one strain gauge, including several finite elements, were taken for comparison.

The maximum stress criterion was adopted as the failure criterion. It states that the laminate layer fails when at least one of the stresses in the laminate reaches the corresponding strength obtained from material tests. Expressing this criterion with the equation, failure occurs when:

$$\sigma_X > F_{xT} \quad \text{for } \sigma_X > 0, x = \{1, 2, \ldots, 6\} \tag{4.1}$$

$$\sigma_X < F_{xC} \quad \text{for } \sigma_C > 0, x = \{1, 2, \ldots, 6\} \tag{4.2}$$

where: σ_X– stress value, F_{xT} – tensile strength of the composite in the x direction, F_{xC} – compressive strength of the composite in the x direction.

FEM models of the tested columns are shown in Fig. 8.

Validation of the numerical model of the columns was carried out in two stages. In the first stage, the correctness of the model was tested by comparing the deformation characteristics obtained from experimental tests of columns in a natural scale with the characteristics determined based on the developed FEM numerical model. The basic criterion adopted in validating the model was the consistency of the F-Δ curves. In addition, in order to verify the FEM numerical model in assessing the behaviour of the columns in the zone near the inspection hole, i.e. in the place where in all cases, the columns were damaged, in the second stage, the stress values in the walls of the columns around the inspection hole were compared. The wall stresses measured during the tests using electro-resistance strain gauges were compared with the deformation values at the same points, determined on the basis of a numerical model.

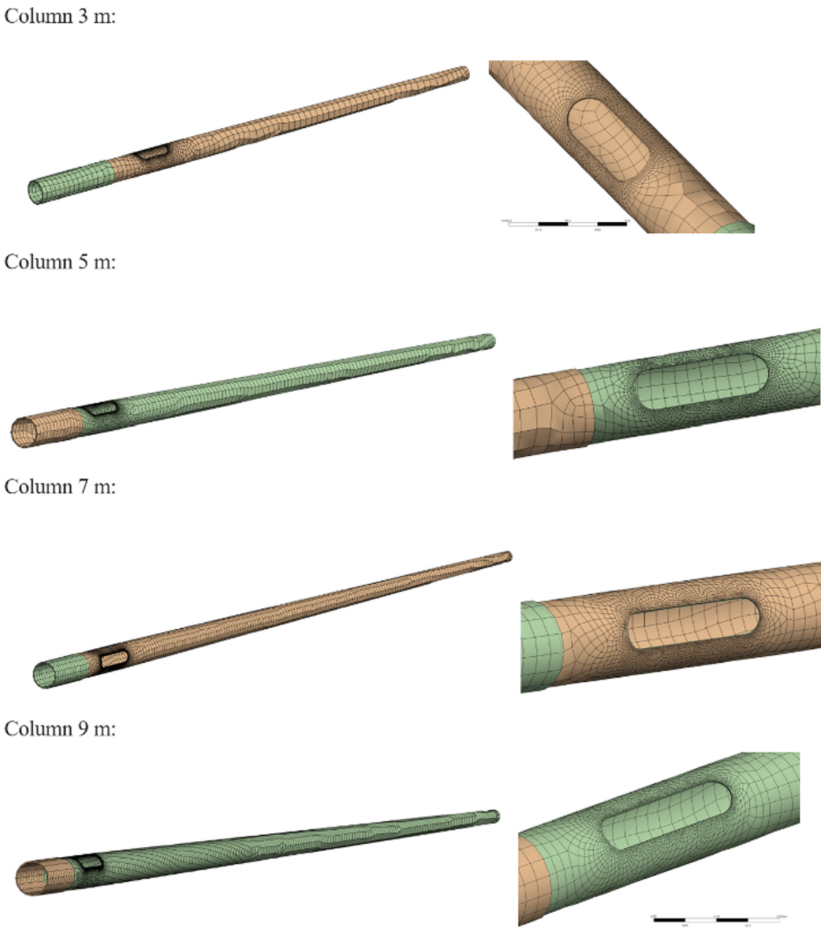

Fig. 8. FEM models of the tested columns

The variables that affected the load capacity of the columns were divided into two categories: constant, whose value remained constant throughout the experiment and whose impact was not evaluated, and variable, whose impact was evaluated. The constant parameters during the tests were the compressive strength of the column material f_y and the height of the column h. The input variables affecting the method of failure and the column load-bearing capacity were: column diameter in the middle of the height of the inspection opening d, inspection hole height L, width of the inspection opening b, rounding radius of the inspection opening corner N, column wall thickness at the inspection opening t, element stiffness modulus E. The output variable parameter was the bending resistance of column $M_{(ux,\mathrm{FEM})}$.

The parameters mentioned above and their values were used to plan a numerical experiment using the FEM software. The specimens with the values of variable parameters determined using the experiment plan were examined. The central rotational compositional plan with

star points was chosen as the experiment plan. The orthogonality alpha of $\alpha = 1.78$ was used to determine the star points. The plan contained two systems in its centre [16]. With six variable parameters, the number of obtained points (copies) of the experiment is 46. Due to the numerical nature of the experiment, repetitions were excluded from the plan because they would give identical results. Using a star points experiment design causes some instances to have variable parameter values outside the assumed range of values. However, these values are still possible to obtain with the numerical model of the column, and their use will improve the quality of the experiment results.

The modes of column failure and their bending resistances were identified as a result of the parametric analysis performed using the column's FEM model. Examples in the experiment plan with physically impossible parameters were changed; in this case, the value $N = b/2$ was used.

In order to examine the compliance of the characteristics of the curves $(F - \Delta)$ obtained experimentally and using a numerical model, parametric and non-parametric tests were performed. For variables with a normal distribution in each group, an F test and a Student's t-test were performed. To determine whether the distribution was normal, the Shapiro-Wilk (SW-W) test was used. The remaining cases were verified by non-parametric tests using the Mann-Whitney U-test. According to the testing assumptions, there are no significant differences between the curves if the p-value from the Student's t-test or the Mann-Whitney U-test is higher than the specified level of significance $\alpha = 0.05$. In the case of the tested curves, in almost all cases the p-value was higher than the assumed level of significance $\alpha = 0.05$. Therefore, with 95% probability it can be state that the characteristics illustrating the deformation of the tested columns under load obtained using the developed numerical model do not differ significantly from the results obtained experimentally. The results of the statistical analysis are presented in Table 6.

Table 6. Testing the compliance of force-displacement curves $(F - \Delta)$ obtained experimentally and those obtained from the FEM model [17]

Column	SW-W; p ANSYS	SW-W; p EXP	Statistic F	p	Test t-Student	p
3-1	0,942; 0,288	0,952; 0,431	1,112	0,825	–0,010	0,496
3-2	0,952; 0,422	0,968; 0,741	1,020	0,967	0,378	0,354
3-3	0,958; 0,485	0,955; 0,430	1,00	0,996	—0,261	0,350
5-1	0,968; 0,885	0,970; 0,907	1,608	0,443	0,943	0,178
5-2	0,946; 0,426	0,943; 0,381	1,358	0,560	0,861	0,198
5-3	0,953; 0,648	0,957; 0,842	8,573	0,001	3,207	0,002
7-1	0,955; 0,286	0,953; 0,250	1,800	0,141	1,869	0,034
7-2	0,958; 0,503	0,959; 0,525	5,979	0,000	-3,520	0,001
7-3	0,960; 0,471	0,955; 0,362	1,841	0,160	1,7001	0,048
9-1	0,945; 0,563	0,934; 0,424	1,401	0,585	–0,701	0,245
9-2	0,966; 0,715	0,964; 0,672	1,329	0,564	0,855	0,199

Note: Underlined indicates incompatibility.

5. Comparative analysis

For comparative purposes, the results obtained from experimental tests were compared with the results of the characteristic resistance calculated on the basis of european standards. The obtained results are compared in Table 7 with respect to the capacity of the columns in the location of the holes. As can be seen from the presented comparison, in the case of each tested column, its experimentally determined capacity was much lower than the capacity calculated on the basis of the standard [5]. The bending resistance of the columns in the location of the inspection hole obtained experimentally was 2.0 to 3.4 times lower than the bending resistance calculated on the basis of European standards, and the difference in bending capacity decreased with the increase in the height of the columns.

Table 7. Comparison of the bending resistance results obtained experimentally with the results obtained based on the relevant standard [5]

Column number	**Bending resistance according to the EN 40-3-3 standard in the inspection hole $M_{ux,k} = 1.5M_{ux}$ (characteristic value) [N·m]**	**Experimental bending resistance in the inspection hole $M_{ux,exp}$ [N·m]**	$M_{ux,k}$ /$M_{ux,exp}$
3/1	5667	1675.9	3.4
3/2	5115	1535.1	3.3
3/3	5679	1614.7	3.5
5/1	5798	2041.6	2.8
5/2	6365	2386.8	2.7
5/3	6802	2489.3	2.7
7/1	14482	6594.1	2.2
7/2	14066	6239.5	2.3
7/3	12915	6480.2	2.0
9/1	14278	6398.1	2.2
9/2	15973	7756.3	2.1

Additionally, the characteristic bending resistances $M_{ux,k}$ calculated using the current standard procedure [5] is more than 1,7 to 2.8 times greater than the bending resistances determined using the FEM numerical model $M_{(ux,FEM)}$ for columns whose dimensions deviate from those determined by experiment (Table 8).

Table 8. Comparison of the bending resistance results determined using the FEM model with the results obtained based on the relevant standard [5]

FEM Column number	**Bending resistance according to the EN 40-3-3 standard in the inspection hole $M_{ux,k} = 1.5M_{ux}$ (characteristic value) [N·m]**	**FEM model bending resistance in the inspection hole $M_{(ux,FEM)}$ [N·m]**	$M_{ux,k}$ /$M_{(ux,FEM)}$
29	25082	11932	2,10
30	7362	4256	1,73
31	10521	4750	2,21
32	26677	13452	1,98
33	35273	12768	2,76
34	37516	14972	2,51
35	12134	5016	2,42
36	12137	5092	2,38
37	40799	14516	2,81
38	15037	6460	2,33
39	4076	2090	1,95

6. Conclusions

The main objective of the research was to validate the standard method for calculating the load capacity of GFRP composite lighting columns under horizontal loads [5] using experimental and numerical data. The work involved developing a numerical model of GFRP composite columns with an inspection hole validated on the basis of experimental research, taking into account the nonlinear behaviour of the columns before the failure phase, and calculating the bending capacity of GFRP composite lighting columns in accordance with European standard [5].

The tested GFRP lighting poles that are sold on the commercial market have a bending resistance that is significantly higher than what is required by the European standards.. The bending capacity of the tested columns at the base was used in 7% in the case of 3.0 m high columns and in 20% in the case of 9.0 m high columns. The utilization of the capacity of the columns in the location of the opening ranges from 0.11 for 3.0 m columns to 0.51 for 9.0 m high columns. This may indicate a large oversize of the column cross-sections, resulting from the fact that the applicable design standards do not take into account the destruction of the columns. in a weakened cross-section in places of inspection holes.

Then, in accordance with the standard [12], experimental tests were performed on GFRP columns on a natural scale to gather data on the stiffness and load-carrying capacity of GFRP composite columns subjected to static loads and experimentally examine the phenomenon of

loss of column stability in the vicinity of the inspection hole. Eleven lighting poles ranging in length from 3.0 m to 9.0 m were included in the test plan.

The bending resistance values determined through the experiment were compared to those determined using the standard procedure described in the standard [5]. In the vicinity of the inspection hole, the ratio of the experimentally determined bending resistance of the columns to the resistance computed using the European standard was in the range of 0.30 to 0.50, and the difference decreased as the columns' height increased.

The results obtained from the conducted experimental tests were used to validate the developed numerical model of FEM. The material characteristics used in the FEM calculations were adopted based on the results of experimental tests. The first validation stage included examining the compliance of the F–Δ characteristics obtained from experimental tests with characteristics determined based on the developed FEM numerical model. Comparing both characteristics with the use of statistical analysis, a good agreement was found. The second stage of validation was aimed at examining the credibility of the developed numerical model in the zone where the destruction of the column took place, i.e. at the site of the inspection hole. For this purpose, the deformation values measured at selected points around the opening using strain gauges were compared with the deformation values at the same points determined on the basis of a numerical model. The performed parametric and non-parametric statistical tests of both characteristics in accordance with the standard [16] confirmed their good compatibility. It was found that the behaviour of the columns under the applied load described by the numerical model in a sufficiently accurate manner corresponds to the behaviour of the experimentally tested columns. It is demonstrated that the stress curves obtained from laboratory tests and those obtained from the FEM model are consistent because the value of p (test probability) is typically higher than the assumed significance level $\alpha = 0.05$.

By comparing the bending resistances determined based on the FEM numerical model with calculated in accordance with the relevant standard [5] it was discovered that the latter is on average 2 to 3 times greater.

According to the design process analysis presented in Eurocode EN 40-3-3 [5], the inspection hole is only treated as a local cross-section reduction that lowers the yield modulus. The possibility of buckling the walls in the inspection hole area is not considered. This indicates that the typical method for figuring out a composite column's bending resistance has not been modified to account for the actual behaviour of composite columns with inspection openings.

The general conclusions drawn from the experimental and numerical tests conducted show that: (1) the bending resistance of GFRP composite lighting columns is significantly overestimated when assessed in accordance with European standards; and (2) the results of the finite element method are sufficiently accurate when used to develop a numerical model of a composite lighting column with an unreinforced inspection opening for use in both scientific research and design practice.

Acknowledgements

This work was supported by the Polish Ministry of Science and Higher Education (the research projects WI/WB-IIL/12/2019, WZ/WB-IIL/4/2020 and WZ/WB-IIL/2/2023).

References

[1] D. Di Vito, M. Kanerva, J. Järveläinen, A. Laitinen, T., Pärnänen, K. Saari, K. Kukko, H. Hämmäinen, and V. Vuorinen, "Safe and Sustainable Design of Composite Smart Poles for Wireless Technologies", *Applied Sciences,* vol. 10, no. 21, art. no. 7594, 2020, doi: 10.3390/app10217594.

[2] "Lamp Posts", StrunoBet Migacz. [Online]. Available: https://strunobet.com/lamp-posts. [Accessed: 10 May 2023].

[3] M. Broniewicz, E. Broniewicz, K. Dec, and S. Lubas, "Barriers to sustainable composite poles adoption in infrastructure", *Economics and Environment,* vol. 77, no. 2, pp. 27–38, 2021, doi: 10.34659/2021/2/10.

[4] M. Broniewicz, F. Broniewicz, and E. Broniewicz, "A Full-Scale Experimental Investigation of Utility Poles Made of Glass Fibre Reinforced Polymer", *Materials*, vol. 14, no. 23, art. no. 7398, 2021, doi: 10.3390/ma14237398.

[5] EN 40-3-3:2013 Lighting columns Design and verification. Verification by calculation.

[6] E.J. Barbero and I.G. Raftoyiannis, "Local Buckling of FRP Beams and Columns", *Journal of Materials in Civil Engineering,* vol. 5, no. 3, pp. 339–355, 1993, doi: 10.1061/(ASCE)0899-1561(1993)5:3(339).

[7] Z.M. Lin, *Analysis of Pole-Type Structures of Fibre Reinforced Plastics by Finite Element Method*. University of Manitoba, 1995.

[8] D. Polyzois, I.G. Raftoyiannis, and S. Ibrahim, "Finite elements method for the dynamic analysis of tapered composite poles", *Composite Structures*, vol. 43, no. 1, pp. 25–34, 1998, doi: 10.1016/S0263-8223(98)00088-9.

[9] R. Masmoudi and S. Metiche, "Full-Scale Flexural Testing on Fibre-Reinforced Polymer (FRP) Poles", *The Open Civil Engineering Journal*, vol. 1, no. 1, pp. 37–50, 2007, doi: 10.2174/1874149500701010037.

[10] P. Wysmulski, K. Falkowicz, and P. Filipek, "Buckling state analysis of compressed composite plates with cut-out", *Composite Structures*, vol. 274, 2021, doi: 10.1016/j.compstruct.2021.114345.

[11] EN 40-7:2002 Lighting columns Requirements for fibre reinforced polymer composite lighting columns.

[12] EN 40-3-1:2013 Lighting columns – Part 3-1: Design and verification - Specification for characteristic loads.

[13] EN 40-3-2:2014 Lighting columns – Part 3-2: Design and verification - Verification by testing.

[14] M. Sandberg, O. Yuksel, R.B. Comminal, M.R. Sonne, M. Jabbari, M. Larsen, F.B. Salling, I. Baran, J. Spangenberg, J.H. Hattel, "Numerical modeling of the mechanics of pultrusion", in *Mechanics of Materials in Modern Manufacturing Methods and Processing Techniques*, V. Silberschmidt, Ed. Elsevier, 2020, pp. 173–195, doi: 10.1016/B978-0-12-818232-1.00006-0

[15] J. Rakowski and P. Wielentejczyk, "Dynamics of Reissner-Mindlin plate strips by FEM", *Vibrations in Physical Systems,* vol. 20, pp. 250–251, 2002.

[16] STATISTICA v. 13.0. [Online]. Available: https://statistica.software.informer.com/13.0/.

[17] ISO 2602:1980 Statistical interpretation of test results - Estimation of the mean - Confidence interval.

Eksperymentalna i numeryczna weryfikacja normowej procedury wyznaczania nośności kompozytowych słupów oświetleniowych GFRP

Słowa kluczowe: analiza MES, badania eksperymentalne, procedura projektowania, słupy oświetleniowe z GFRP

Streszczenie:

Głównym celem pracy była weryfikacja naukowa obliczeniowej procedury normowej, umożliwiającej projektowanie słupów GFRP o przekroju kołowym, wykonanych z tworzywa polimerowego wzmocnionego włóknem szklanym, poddanych obciążeniom poziomym. W celu osiągnięcia zamierzonego rezultatu opracowano model numeryczny słupów kompozytowych GFRP z otworem rewizyjnym uwzględniający nieliniowe zachowanie się słupów poprzedzające fazę zniszczenia. Weryfikację opracowanego modelu numerycznego dokonano poprzez realizację programu eksperymentalnego obejmującego badania doświadczalne 11 słupów oświetleniowych GFRP w skali naturalnej oraz badania materiałowe kompozytu. W pierwszej części pracy zastosowano procedurę normową obliczania nośności oświetleniowych słupów kompozytowych z otworem rewizyjnym według postanowień norm (PN-EN 40-3-3, 2013) oraz

(PN-EN 40-7, 2004) do obliczeń projektowych badanych słupów, wyznaczając ich nośność na zginanie we wszystkich punktach krytycznych oraz wartość ugięcia wierzchołka słupa. Sprawdzono warunki stanu granicznego nośności porównując obliczone nośności z wartościami momentów zginających od obciążenia wiatrem wyznaczonych w przypadku słupów kompozytowych zgodnie z postanowieniami normy (PN-EN 40-3-1, 2014) oraz warunki stanu granicznego użytkowalności, porównując ugięcia poziome słupów w miejscu przyłączenia latarni z wartościami dopuszczalnymi. Stwierdzono, że wykorzystanie nośności badanych słupów w miejscu otworu rewizyjnego wynosi od 5% w przypadku słupów o wysokości 3,0 m do 55% w przypadku słupów o wysokości 9,0 m, natomiast przemieszczenie wierzchołka badanych słupów we wszystkich przypadkach jest mniejsze od wartości dopuszczalnych. Następnie przedstawiono badania doświadczalne słupów GFRP w skali naturalnej przeprowadzone zgodnie z normą (PN-EN 40-3-2, 2014), których celem było uzyskanie danych doświadczalnych dotyczących nośności i sztywności słupów kompozytowych GFRP poddanych obciążeniom statycznym oraz eksperymentalne zbadanie zjawiska utraty stateczności trzonu słupa w sąsiedztwie otworu rewizyjnego. Plan badań obejmowałjedenaście słupów oświetleniowych o długościach od 3,0 m do 9,0 m. Analizowano cztery formy zniszczenia słupów: w obszarze otworu rewizyjnego, przy podstawie, w obszarze poza otworem rewizyjnym oraz utratę stateczności miejscowej w wyniku owalizacji przekroju. We wszystkich badanych słupach wystąpiła ta sama forma wyczerpania nośności słupa polegająca na zniszczeniu trzonu w obszarze otworu. Dokonano również porównania wartości nośności otrzymanych z badań doświadczalnych z wynikami uzyskanymi na podstawie obliczeń według normy przedmiotowej. W przypadku wszystkich badanych słupów ich nośność stwierdzona doświadczalnie była znacznie mniejsza i stanowiła od 28% do 50% nośności obliczeniowej wyznaczonej na podstawie normy przedmiotowej. Wyniki uzyskane z przeprowadzonych badań doświadczalnych posłużyły do dwuetapowej walidacji opracowanego modelu numerycznego słupów MES. Charakterystyki materiałowe wykorzystane w obliczeniach MES przyjęto na podstawie wyników badań doświadczalnych. Pierwszy etap walidacji obejmowałzbadanie zgodności przebiegu charakterystyk F–Δ uzyskanych z badań doświadczalnych z charakterystykami wyznaczonymi na podstawie opracowanego modelu numerycznego MES. Dokonując porównania obu charakterystyk przy pomocy analizy statystycznej stwierdzono dobrą ich zgodność. Drugi etap walidacji miał na celu zbadanie wiarygodności opracowanego modelu numerycznego w strefie, gdzie następowało zniszczenie słupa, tzn. w miejscu otworu rewizyjnego. W tym celu porównano wartości odkształceń pomierzone w wytypowanych punktach wokółotworu przy użyciu tensometrów z wartościami odkształceń w tych samych punktach określonych na podstawie modelu numerycznego. Przeprowadzone testy parametryczne i nieparametryczne obu charakterystyk zgodnie z normą (PN-ISO 2854:1994). potwierdziły ich dobrą zgodność. W efekcie porównania wyników przemieszczeń końca słupa oraz wartości odkształceń w sąsiedztwie otworu rewizyjnego uzyskanych w sposób doświadczalny oraz przy pomocy MES wykazano, że zachowanie się słupów pod przyłożonym obciążeniem opisywane przez opracowany model numeryczny w sposób wystarczająco dokładny odpowiada zachowaniu się słupów badanych doświadczalnie. Ostatnia część artykułu zawiera porównanie wyników nośności na zginanie otrzymanych na podstawie badań doświadczalnych, badań numerycznych MES oraz obliczonych zgodnie z obecnie obowiązującą procedurą normową. Porównując nośności na zginanie wyznaczone na podstawie modelu numerycznego MES oraz badań doświadczalnych z obliczonymi zgodnie z odpowiednią normą stwierdzono, że nośność oświetleniowego słupa kompozytowego GFRP obliczona według normy EN 40-3-3 jest ponad 2,5 razy większa od nośności stwierdzonej doświadczalnie i numerycznie. Zgodnie z analizą procesu projektowania przedstawioną w Eurokodzie EN 40-3-3 otwór rewizyjny traktowany jest jedynie jako lokalne zmniejszenie przekroju poprzecznego, które obniża moduł sprężystości. Nie uwzględnia się możliwości wyboczenia ścian słupa w rejonie otworu rewizyjnego. Oznacza to, że typowa metoda obliczania nośności słupa zespolonego na zginanie nie została zmodyfikowana w celu uwzględnienia rzeczywistego zachowania słupów zespolonych z otworami kontrolnymi.

Received: 2023-10-28, Revised: 2024-01-18